# Fallout plume of submerged oil from *Deepwater Horizon*

David L. Valentine[a,b,1], G. Burch Fisher[a,b], Sarah C. Bagby[a,b], Robert K. Nelson[c], Christopher M. Reddy[c], Sean P. Sylva[c], and Mary A. Woo[d]

[a]Department of Earth Science and [b]Marine Science Institute, University of California, Santa Barbara, CA 93106; [c]Department of Marine Chemistry and Geochemistry, Woods Hole Oceanographic Institution, Woods Hole MA 02543; and [d]Department of Earth System Science, University of California, Irvine, CA 92697

Edited by Derek C. G. Muir, Environment Canada, Burlington, ON, Canada, and accepted by the Editorial Board September 26, 2014 (received for review August 5, 2014)

**The sinking of the *Deepwater Horizon* in the Gulf of Mexico led to uncontrolled emission of oil to the ocean, with an official government estimate of ∼5.0 million barrels released. Among the pressing uncertainties surrounding this event is the fate of ∼2 million barrels of submerged oil thought to have been trapped in deep-ocean intrusion layers at depths of ∼1,000–1,300 m. Here we use chemical distributions of hydrocarbons in >3,000 sediment samples from 534 locations to describe a footprint of oil deposited on the deep-ocean floor. Using a recalcitrant biomarker of crude oil, 17α(H),21β(H)-hopane (hopane), we have identified a 3,200-km$^2$ region around the Macondo Well contaminated by ∼1.8 ± 1.0 × 10$^6$ g of excess hopane. Based on spatial, chemical, oceanographic, and mass balance considerations, we calculate that this contamination represents 4–31% of the oil sequestered in the deep ocean. The pattern of contamination points to deep-ocean intrusion layers as the source and is most consistent with dual modes of deposition: a "bathtub ring" formed from an oil-rich layer of water impinging laterally upon the continental slope (at a depth of ∼900–1,300 m) and a higher-flux "fallout plume" where suspended oil particles sank to underlying sediment (at a depth of ∼1,300–1,700 m). We also suggest that a significant quantity of oil was deposited on the ocean floor outside this area but so far has evaded detection because of its heterogeneous spatial distribution.**

Macondo Well blowout | Gulf of Mexico | ocean pollution | petroleum spill | deep plumes

The sinking of the *Deepwater Horizon* in the Gulf of Mexico led to the discharge of ∼5.0 million barrels of petroleum from the Macondo Well. The discharge occurred at a water depth of ∼1,500 m and gave rise to intrusion layers (1) in the deep ocean that included both water-soluble hydrocarbons in the dissolved phase (2–6) and small particles of water-insoluble hydrocarbons (7–11). These intrusion layers were found primarily at a depth of 1,000–1,300 m and may have hosted the majority of the environmental discharge, including all the natural gas and ∼2 million barrels of liquid oil (12). Although the most abundant of the water-soluble hydrocarbons underwent rapid biodegradation during the spill (4, 6, 8, 9, 13–15), the fate and impacts of the insoluble hydrocarbons in the deep ocean have remained uncertain (16).

The intrusion layers that hosted hydrocarbon contamination persisted for 6 mo or more and at distances >300 km from the well, but available evidence suggests that particles of submerged oil were particularly concentrated during the first 6 wk of discharge and within ∼15 km of the well (8, 9, 11). Thus, initial partitioning of hydrocarbon particles to the intrusion layers appears to have given way to transport or removal by undefined deep-ocean processes. Such processes might include sedimentation, buoyant rise toward the sea surface, incorporation into pelagic biota, biodegradation, or interventions at the wellhead. Mechanisms exist that support several of these options (9, 17–20), but uncertainty as to oil's actual partitioning, the effect of chemical dispersant (21), and the impacts of a changing microbial community (6, 8, 9, 13–15, 17, 22–24) have precluded further understanding of the processes that acted on the oil.

In this study we focus on testing the hypothesis that oil particles suspended in the deep intrusion layers were deposited on the sea floor over a broad area. To do so, we use publicly available data generated as part of the ongoing Natural Resource Damage Assessment (NRDA) process (*Supporting Information*) to assess the spatial distribution of petroleum hydrocarbons in the deep-ocean sediments of the Gulf of Mexico. We focus on the recalcitrant compound 17α(H),21β(H)-hopane (hereafter referred to as "hopane") as a conserved tracer for crude oil deposition to sediments (25); we treat hopane as a degradation-resistant proxy for Macondo's liquid-phase oil (26). Analysis of the spatial distribution of hopane allows us to define both a regional background level and a depositional footprint of oil from the *Deepwater Horizon* event. In combination with other lines of evidence, this analysis leads us to conclude that significant quantities of particulate oil sank from the intrusion layers to rest on the underlying sea floor.

## Results and Discussion

**Hopane Distribution Is Consistent with Macondo as the Source.** Our first goal was to determine if the distribution of hopane in the Gulf of Mexico's deep-water sediments could be used quantitatively as a tracer of Macondo discharge. Because hopane is not unique to Macondo Well oil, we investigated its spatial distribution (Fig. 1) for indications of its origin. To help determine

### Significance

**Following the sinking of the *Deepwater Horizon* in the Gulf of Mexico an unprecedented quantity of oil irrupted into the ocean at a depth of 1.5 km. The novelty of this event makes the oil's subsequent fate in the deep ocean difficult to predict. This work identifies a fallout plume of hydrocarbons from the Macondo Well contaminating the ocean floor over an area of 3,200 km$^2$. Our analysis suggests the oil initially was suspended in deep waters and then settled to the underlying sea floor. The spatial distribution of contamination implicates accelerated settling as an important fate for suspended oil, supports a patchwork mosaic model of oil deposition, and frames ongoing attempts to determine the event's impact on deep-ocean ecology.**

Author contributions: D.L.V., R.K.N., C.M.R., S.P.S., and M.A.W. designed research; D.L.V., G.B.F., and S.C.B. analyzed data; and D.L.V. wrote the paper.

The authors declare no conflict of interest.

This article is a PNAS Direct Submission. D.C.G.M. is a guest editor invited by the Editorial Board.

Freely available online through the PNAS open access option.

[1]To whom correspondence should be addressed. Email: valentine@geol.ucsb.edu.

This article contains supporting information online at www.pnas.org/lookup/suppl/doi:10.1073/pnas.1414873111/-/DCSupplemental.

whether hopane originated from the Macondo Well, we asked whether its distribution was consistent with the *Deepwater Horizon* event across three spatial scales. That is, for a given core, is the hopane concentration higher in the surficial layer of sediment than in underlying sediment, as would be expected for recent deposition? For a given sampling site, do surficial hopane concentrations vary widely from core to core, as would be expected for particle deposition? For the region, is hopane concentration elevated close to the Macondo Well, as might be expected for proximity to an intense point source?

To assess whether hopane in surficial sediments (i.e., the uppermost 1 or 2 cm of the sediment that makes up the sea floor) originated from recent deposition, we assessed its depth distribution in sediment cores for which complete depth profiles were available. Cores were binned by expedition to retain consistent sample intervals; data were normalized to the surface layer (=100%) for each core and binned by surficial hopane concentration to establish a baseline trend (*Supporting Information*). Cores with surficial hopane concentrations of <25 ng·g$^{-1}$ show a slight linear decrease in hopane concentration with sediment depth, providing no indication of recent deposition, but the hopane profile in cores with higher surficial concentrations is best fit by an exponential decay curve (Fig. 2), suggesting recent anomalous hopane deposition in these cores. The 323 cores with the highest (>100 ng·g$^{-1}$) levels of surficial hopane, collected during eight expeditions, follow this pattern with notable consistency (Fig. 2*A*).

Next, we examined the variability of surficial hopane concentrations in sets of cores collected in parallel. These measurements frequently ranged over one to two orders of magnitude at a single sampling site (Fig. S1). We used surficial hopane concentrations to develop a quantitative particle deposition model and asked whether the model could explain the high degree of variation observed. Because little is known of the likely distribution of oil masses carried by depositing particles, we used Monte Carlo methods to fit particle number and oil mass to the measured distribution of surficial hopane concentration (Figs. S2 and S3). This multimodal distribution was best fit by deposition at a spatial density of 228 particles/m$^2$, with 88% of particles bearing an average (unweathered) oil mass of 0.024 g each, 10% bearing an average oil mass of 0.19 g, and 2% bearing an average oil mass of 1.13 g (mean hopane masses of 1.4, 11, and 65 μg, respectively; see *Supporting Information* for details). We then used this model to simulate 2 m × 2 m patches of seafloor, selected two to five positions at random in each patch for "coring," and calculated (*i*) the surficial hopane concentration that would result from the particles deposited within each simulated core's cross-section and (*ii*) the mean and SD of these concentrations for each simulated site. Finally, for each sample site in the Gulf of Mexico at which parallel cores were collected, we calculated the mean and SD of measured surficial hopane concentrations. The within-site variation as measured in parallel cores was in very good agreement with simulated values (Fig. 3), indicating that sparse deposition of heterogeneous oil-bearing particles is sufficient to explain the frequent coexistence of highly contaminated spots alongside spots with low hopane concentration.

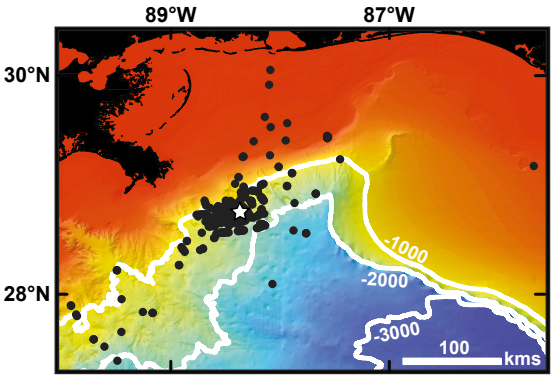


**Fig. 1.** Map of the northern Gulf of Mexico showing the sampling locations (black dots) and the Macondo Well (white star) overlaid on the National Geophysical Data Center Coastal Relief Model bathymetry.

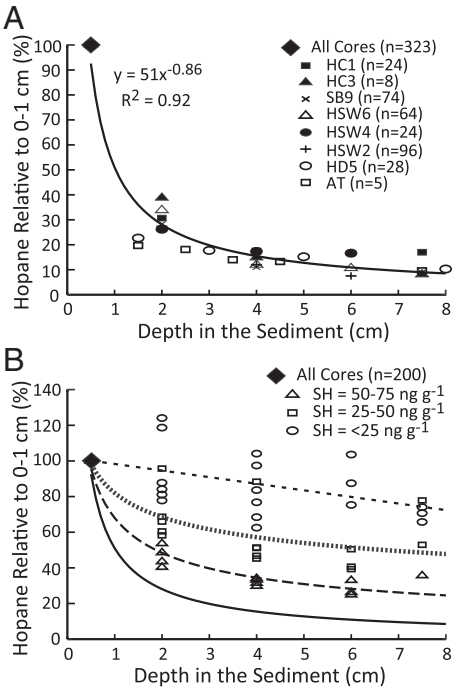


**Fig. 2.** Depth distributions of hopane concentration. (*A*) Hopane's depth distribution relative to the surficial layer (0–1 cm) for sediments with surficial hopane (SH) >100 ng·g$^{-1}$. The data are given as the midpoint depth for each sediment interval and as the mean value for each sampling expedition as indicated. (*B*) Hopane's depth distribution relative to the surficial layer (0–1 cm) for sediments with surficial hopane concentrations of <25 ng·g$^{-1}$, 25–50 ng·g$^{-1}$, and 50–75 ng·g$^{-1}$. The data are in the same form as in *A*. Regressions are fit to the data, from top to bottom, as follows: SH <25 ng·g$^{-1}$ ($y = -3.7x + 102$; $R^2 = 0.31$); SH = 25–50 ng·g$^{-1}$ ($y = 82x^{-0.26}$, $R^2 = 0.62$); SH = 50–75 ng·g$^{-1}$ ($y = 68x^{-0.49}$, $R^2 = 0.93$). The solid curve at bottom (SH >100 ng·g$^{-1}$) is from *A* and is provided for visual reference. Additional information is available in Dataset S1.

To assess whether surficial hopane was elevated in the vicinity of the Macondo Well, we analyzed its spatial distribution for all available locations as a function of the radial distance from the Macondo Well and the sea floor depth. The results shown in Fig. 4 and Fig. S4 indicate a mean concentration for surficial hopane of 28 ± 23 ng·g$^{-1}$ ($n$ = 70) for locations >40 km from the Macondo Well, providing an estimate for the mean background concentration (see *Supporting Information* for additional details). Only 3% of sampling sites at this distance from the well contained surficial hopane concentrations >75 ng·g$^{-1}$ (Fig. 4*A* and Fig. S4), whereas 68% (314 of 464) of locations within 40 km of the Macondo Well contained surficial hopane at >75 ng·g$^{-1}$, providing an estimate for the upper limit of background concentrations. The concentration of surficial hopane depended on sea floor depth (Fig. 4 *B* and *C*), with peak values at 1,300–1,600 m, bracketed by lower but still elevated concentrations at 900–1,300 and 1,600–1,700 m. Outside these depths and within 40 km of the Macondo Well only 17% of locations (9 of 54) contained surficial hopane concentrations >75 ng·g$^{-1}$, compared with 74% of samples (303 of 410) within this depth range and within 40 km of the Macondo Well. This basin-scale analysis provides an

ENVIRONMENTAL SCIENCES

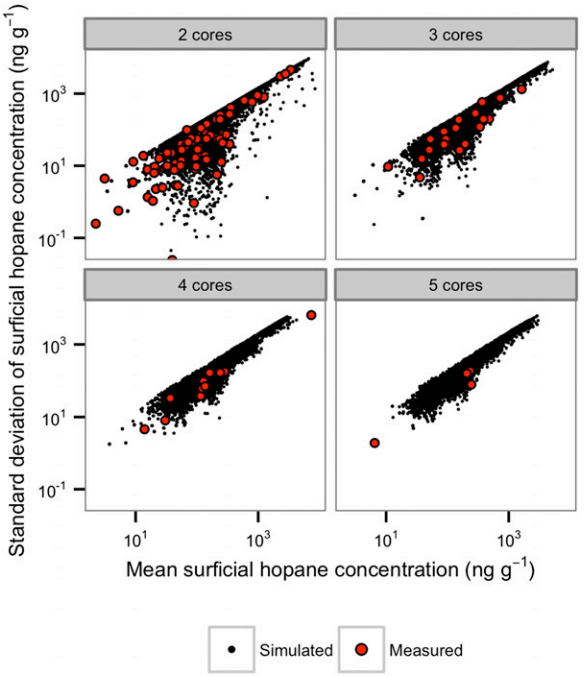


**Fig. 3.** Comparison of measured variation in surficial hopane concentrations within sampling sites (red dots) and modeled variation within simulated sampling sites (black dots). Within-site variability was assessed in the particle deposition model by simulating deposition on a patch of sediment, randomly sampling two, three, four, or five nonoverlapping loci with the same cross-sectional area as standard push-cores, calculating the hopane signal that would result from the combination of background signal and oil particles captured within each locus, and comparing the results across loci within the same simulated site.

estimate of 28 ng·g$^{-1}$ for the mean background concentration of surficial hopane and a threshold of 75 ng·g$^{-1}$ for distinguishing between background surficial hopane and hopane contamination and further defines a clear regional anomaly that is highly pronounced within 40 km of the Macondo Well and at depths of 900–1,700 m.

Collectively, these analyses of the distribution of hopane concentration in the Northern Gulf of Mexico across multiple spatial scales suggest a recent, intense, and heterogeneous depositional event centered near the Macondo Well. Based on this evidence and the magnitude of discharge during the event, we attribute the excess hopane observed in surficial sediments to discharge from the Macondo Well and propose that this hopane anomaly be used as a proxy for liquid oil from the spill.

**Extent and Pathway of Hopane Deposition.** The second goal of this study was to quantify the depositional footprint of the spill and identify pathways by which the oil might have deposited. Toward this goal we posed several questions. What fraction of hopane discharge resides in the contaminated zone? Is the spatial distribution of surficial hopane contamination consistent with a source from the deep intrusion layers? Does the pattern of contamination provide insight as to the oil's depositional pathway?

To estimate the magnitude of emitted hopane deposited to the sea floor within the defined contaminated area, we used multiple approaches (Tables S1–S4) to interpolate the total surficial hopane contamination load from surficial hopane concentration measurements. With the assumption that the mean background concentration is 28 ± 23 ng·g$^{-1}$, our preferred method of calculation yields a total load for surficial hopane contamination of 1.8 ± 1.0 × 10$^6$ g, which represents ∼6 ± 5% of the hopane emitted to the environment from the Macondo Well; we take the lowest estimate minus one SD as a lower bound and the highest estimate plus one SD as an upper bound, yielding a range of 0.7 × 10$^6$ to 3.4 × 10$^6$ g. Assuming that 2 ± 0.2 million barrels of oil remained trapped at depth (12), these calculations represent, by proxy, ∼12% (range, 4–31%) of the oil trapped in the deep intrusion layers. We view this estimate as a lower bound for the region investigated because three reservoirs of hopane contamination are missing from the calculation: (*i*) sediments beneath the surficial layer (Fig. 2*B*); (*ii*) the water overlying core samples upon collection; and (*iii*) sediments in the debris field that include splays of drilling mud from the failed top-kill operation. Furthermore, the identified contamination represents a minimum area, because the spatial extent was truncated for areas of low sample density. Because hopane is used as a proxy for oil, the estimate does not account for biodegradation or dissolution of other petroleum hydrocarbons.

To assess further the spatial distribution of hopane contamination, we contoured the concentration of surficial hopane in an area of 3,200 km$^2$ for which we had sufficient data coverage ($n$ = 461 locations). Fig. 5 displays results from an empirical Bayesian kriging method (other methods provided similar results; see *Supporting Information*) and reveals an oblong patchwork of contamination that trends primarily to the west from the Macondo Well to a distance of at least 40 km. The observed pattern is consistent with the mixing and deep-ocean currents during the event (24, 27, 28), although we identified less oil to the east than would be expected from current patterns. Comparing the observed deposition pattern with the region's bathymetry reveals moderate hopane contamination along the continental slope at sea floor depths of 900–1,300 m, the depths at which hydrocarbon intrusion layers were reported (2–4, 7, 9), and a stronger hopane anomaly at depths of 1,300–1,600 m (Figs. 4 and 5). Although the contamination at 900–1,300 m is consistent with a bathtub-ring mechanism of deposition, the heavier contamination below suggests that fallout from the intrusion layers was more important. The observed distribution of hopane contamination implicates the intrusion layers rather than the sea surface as the likely source of oil to deep-ocean sediments.

To distinguish better between deposition from the intrusion layers and deposition from the sea surface, we used hopane's distribution to anchor analysis of two other datasets: the footprint for surface oil slicks as observed by remote sensing during the time of discharge (29) and the spatial distribution of several volatile hydrocarbons present at contaminated locations. These datasets have the potential to discriminate between two possible modes of deposition: mode 1, sedimentation of oil that was released from the Macondo Well and trapped in the ocean's interior without ever being exposed to the atmosphere; and mode 2, sedimentation of Macondo oil from the sea surface to the sea floor [the sinking of oil-laden particles from the sea surface popularly referred to as "the dirty blizzard" (16), by analogy with natural marine snow]. We first compared the footprint of the observed hopane anomaly with the footprint for surface oil slicks. Together with rapid surface transport (30, 31) and slower transport of the deep plumes (32), the profound mismatch in these footprints (Fig. 6*A*) argues against the sea surface (mode 2) as the major source of deposition. We then analyzed the spatial distribution of several volatile hydrocarbons present at a subset of contaminated locations (i.e., with surficial hopane concentrations >75 ng·g$^{-1}$). Volatile hydrocarbons are lost to evaporation rapidly when oil is exposed to the atmosphere; thus, the presence of undecane (Fig. S5) and hexadecane (Fig. 6*B*) at 51 and 65 of these locations, respectively, indicates that oil in these samples was not exposed to extensive weathering in surface slicks (10), again arguing against mode 2 deposition. Similarly, the ratio of pristane to phytane (1.63–1.99 in Macondo oil) (5, 33) drops with extensive weathering; previous work with Macondo oil has found values as low as 1.16 for moderately weathered

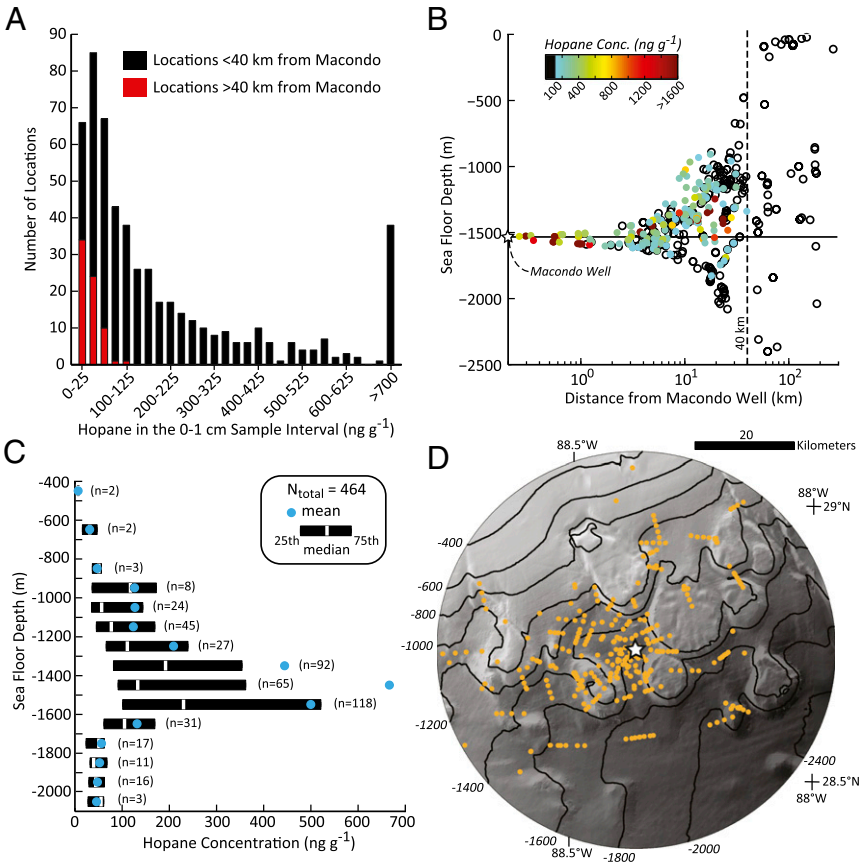


**Fig. 4.** Spatial distribution and concentrations of hopane in surficial sediments. (*A*) Histogram of all surficial hopane samples ($n$ = 534) binned by concentration. (*B*) Plot of data from *A* with respect to sea floor depth and distance from the Macondo Well and colored by hopane concentration. Twenty-one samples have concentrations >1,600 ng·g$^{-1}$ with a maximum concentration of 12,800 ng·g$^{-1}$. (*C*) Box plot showing the depth distribution of surficial hopane concentration for all locations within a 40-km radius of the Macondo Well. The median (white bars), mean (blue dots), and 25th and 75th percentile confidence limits (black box) are shown for samples binned by 100-m sea floor depth intervals. (*D*) Map view of all sample locations within 40 km of the Macondo Well (orange dots and white star, respectively) as plotted in *C*, with 200-m bathymetry contour intervals shown (black lines).

slicks (33), 0.11 for thin slicks after several hours of weathering (34), and 0.29 for floating debris (35). We determined the pristane:phytane ratio for the 84 available locations, finding a median value of 1.68 (mean = 2.2, SD = 1.8), with only one value below 0.97. The similarity between these ratios and the value for Macondo oil again suggests mainly mode 1 deposition. None of the lines of evidence presented here absolutely excludes a contribution from mode 2 deposition, but all support the claim that the observed hopane anomaly (Fig. 5) was derived primarily from the fraction of Macondo oil that initially was suspended as intrusion layers in the ocean's interior.

**Implications and Mechanisms.** The results of this work identify a fallout plume of hopane from the *Deepwater Horizon* event that spans an area of 3,200 km$^2$ and by proxy represents 4–31% of the oil estimated to have been trapped in the deep ocean. Beyond this finding, the results carry several notable implications and provide insight as to the mechanism of mode 1 oil deposition.

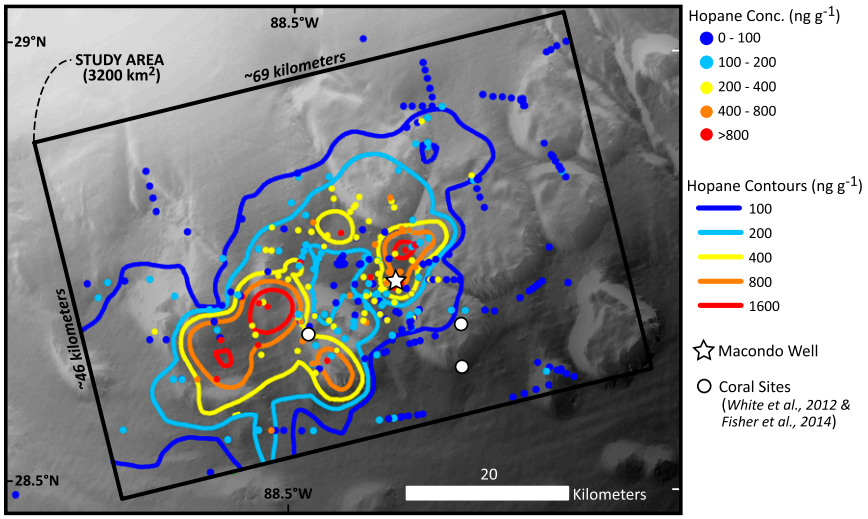


**Fig. 5.** Interpolated hopane contours generated using empirical Bayesian kriging (EBK) for surface C (EBK-C; Figs. S6–S8 and Table S4) and overlaid on measured hopane concentrations and regional bathymetry (see *Supporting Information* for details of the interpolation parameters and techniques).

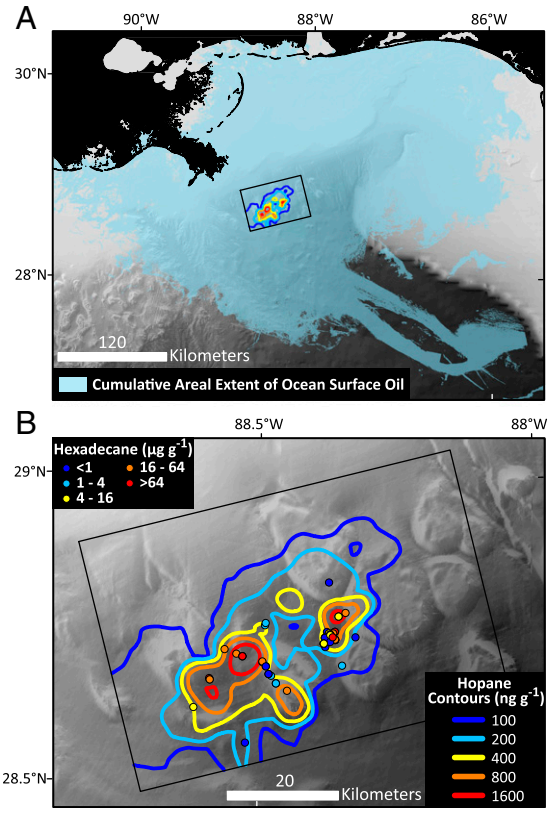


**Fig. 6.** Spatial and chemical evidence supporting mode 1 deposition. (*A*) Cumulative areal extent of ocean surface oil (blue) detected using Synthetic Aperture Radar with a Textural Classifier Neural Network Algorithm (TCNNA) from April to mid-August, 2010 (29). The study area and hopane contours from Fig. 5 are shown along with bathymetry and the Gulf Coast (black). (*B*) Concentration of hexadecane overlaid on the interpolated hopane contours and study area from Fig. 5 ($n$ = 65).

The combination of a patchy distribution at the regional scale (Fig. 5 and Figs. S6–S8) with the heterogeneity observed at the meter-long scale (Fig. 3 and Figs. S1–S3) lead us to a conceptual view of the oil's distribution as a patchwork mosaic. This framework provides hints about the location of as yet unidentified deposits. That is, based on a model of settling oil particles or floc (17, 20), we predict that deposition of similarly sized particles occurred over an area much greater than 3,200 $km^2$, but that the average distance between deposited particles increased in proportion to the radial arc from the Macondo Well. Increased distance between deposited particles would reduce the probability of finding Macondo oil within any given sediment core, so that the sparser sampling performed away from the wellhead is unlikely to have captured the full extent of contamination.

For oil to sink from the deep intrusion layers to the sea floor, oil particles must overcome the ambient hydrodynamic forces holding them in suspension, most likely by increasing in size and density. What process(es) might cause these changes? A mechanism for accelerated settling has yet to be defined adequately but must differ from processes at the sea surface (20), because suspension at depth precludes both evaporative weathering and accumulation at an air–sea interface. The results presented here do not define a mechanism, but in combination with the published literature (6, 8, 9, 15, 17, 36) they lead us to hypothesize that bacterial blooms driven primarily by consumption of soluble hydrocarbons produced biomass that acted as flocculant to capture suspended hydrocarbon particles. Oily bacterial flocs could have increased in size by accretion and/or continued bacterial growth on aqueous-phase hydrocarbons; floc density could have increased by this accumulation of dense bacterial biomass/biofilms combined with the selective biodegradative loss of lighter hydrocarbons from the particulate phase. Estimations of particle oil content indicate the accretion of $10^4$–$10^7$ smaller particles (with an initial size of 50–100 μm) before sinking (Table S5). This mechanism of accelerated settling fulfills both the size and density requirements, is consistent with the flocculation of *Colwellia* (17), and generally is consistent with the patchwork mosaic model of deposition. Such aggregation seemingly counters the effect of dispersant, and the underlying mechanism remains a speculative unknown. Based on this hypothesis we suggest that feedback between microbial blooms and oil deposition could have modulated the intensity and location of deposition.

The spatial distribution of above-background surficial hopane defines a contaminated area that frames interpretations of the resulting ecological damage. For example, potentially damaged deep-sea corals (37) lie within the contaminated region to the southwest of the Macondo Well (Fig. 5). Our analyses indicate that significant quantities of Macondo oil were transported near the corals before or during fallout to the sediment. Deposition of oil in the vicinity of the coral community provides a route to exposure, which has been a topic of contention (37–39). Two additional impacted coral communities (40) to the southeast also lie within the contaminated region (Fig. 5). As a second example, the ecological damage to soft-bottom benthic communities (e.g., a reduction in macrofaunal and meiofaunal diversity and an increase in the nematode-to-copepod ratio) from Macondo oil might mirror the patchwork mosaic pattern of contamination. Accepted approaches to assess ecological damage to the deep benthos include collecting chemical and ecological data from parallel cores. However, the mosaic pattern of oil deposition may complicate such an assessment because of the heterogeneity expected at this spatial scale (Fig. 3 and Fig. S1). We predict this mosaic effect would become more pronounced as particle spatial density decreases with increasing distance from the Macondo Well, potentially explaining why such ecological impacts are more clearly apparent at close proximity to the well (41).

Finally, the identification of hopane contamination from *Deepwater Horizon* in surficial sediments provides a conservative benchmark to which other hydrocarbons can be compared. This approach provides a path to study the physical processes that acted on the oil particles and to assess in situ rates of hydrocarbon biodegradation.

## Methods

The data used in this study were collected and released through the NRDA process, overseen by the National Oceanic and Atmospheric Administration (NOAA). All data are publicly available from NOAA and were downloaded on January 1, 2014 from www.gulfspillrestoration.noaa.gov/oil-spill/gulf-spill-data/. We included all samples from the offshore environment available for download by January 1, 2014. We then selected the subset of samples that included data for hopane concentration measured in the surficial sediment (top 1 or 2 cm, referred to here as "surficial hopane"). A total of 549 stations met this criterion for inclusion. We excluded 15 of these stations because the concentration of hopane increased markedly with depth, indicating long-term inputs consistent with natural oil seepage, although this approach is conservative and may exclude physically mixed samples containing Macondo oil. Replicate samples were collected at 117 of the 534 stations as follows: two samples were collected at each of 81 stations, three samples were collected at each of 21 stations, four samples were collected at each of 11 stations, and five samples were collected at each of four stations. For stations where multiple samples were collected, the average value was used to represent the hopane concentration at that station, but samples were considered individually for other analyses. Hopane concentration was below detection in the surficial sediments at 11 of the 534 stations. The samples originated from 12 expeditions as follows: Pisces Cruise 6 (P6; 25 September–5 October 2010); HOS Davis Cruise 3 (HD3; 8–28 September 2010); HOS Davis

Cruise 5 (HD5; 4–18 December 2010); Atlantis Cruise (AT; 4–15 December 2010); HOS Sweetwater Cruise 1 (HSW1; 10–13 March 2011); HOS Sweetwater Cruise 2 (HSW2; 23 March–24 April 2011); Sarah Bordelon Cruise 9 (SB9; 23 May–13 June 2011); HOS Sweetwater Cruise 4 (HSW4; 14 July–7 August 2011); HOS Sweetwater Cruise 6 (HSW6; 24 August–2 September and 29 September–21 October 2011); Holiday Chouest Cruise 1 (HC1; 25 August–13 September 2011); Holiday Chouest Cruise 2 (HC2; 15–30 September 2011); and Holiday Chouest Cruise 3 (HC3; 1–25 October 2011). Stations are identified in Fig. 1 and in *Supporting Information*.

Hopane concentration was measured as nanograms of hopane per gram of dry sediment. To integrate the hopane concentration spatially, we first calculated the average mass of dry sediment per unit volume of total sediment for available samples of the surface layer. Using an average sediment mass fraction (± SD) of 0.31 (± 0.13) ($n$ = 1,091) and a particle density of 2.65 g/cm$^3$ (42), we calculate an average sediment mass of 0.38 ± 0.16 g/cm$^3$ of total sediment. These values equate to a sediment porosity of 0.86 ± 0.06, which is within the range typically observed for sediment core tops in the Gulf of Mexico (43). We then multiplied the specific density value of 0.38 ± 0.16 g/cm$^3$ by the volume of the study area ($3.2 \times 10^{13}$ cm$^2$ × 1 cm depth interval) and the average excess of hopane, $1.51 \pm 0.23 \times 10^{-7}$ g(hop)/g(sed) [range, 1.2–2.0 × $10^{-7}$ g(hop)/g(sed)] to yield a surficial hopane load estimate of $1.8 \pm 1.0 \times 10^6$ g (range, 0.7–3.4 × $10^6$ g). This value was compared with the total environmental discharge of hopane ($3.0 \pm 0.7 \times 10^7$ g; $1.5 \pm 0.4 \times 10^7$ g to the deep intrusion layers) calculated from the estimated environmental release of oil ($5.2 \pm 0.5 \times 10^{11}$ g; $2.5 \pm 0.3 \times 10^{11}$ g for the deep intrusion layers) and the mass fraction of hopane measured in the source oil (58 ± 8 μg hopane/g of oil). The particle number and particle oil mass parameters in the deposition model were fitted using these values and $\chi^2$ minimization against the distribution of measured hopane concentrations from all 707 cores collected at the 534 stations.

**ACKNOWLEDGMENTS.** We thank Christoph Aeppli, Matthias Kellermann, Karin Lemkau, Scott Stout, and J. P. Walsh for useful advice; Deborah French-McCay for preparation and coordination of Natural Resource Damage Assessment (NRDA) cruises; James Payne for coauthoring NRDA cruise plans and leading several cruises; and the National Oceanic and Atmospheric Administration for the use of data collected as part of the NRDA of the *Deepwater Horizon* spill. This work was supported, in part, by National Science Foundation Grants OCE-1333162, OCE-0961725, EAR-0950600, and OCE-1046144 (to D.L.V.), and Grants OCE-1333148 and OCE-0960841 (to C.M.R.).

1. Socolofsky SA, Adams EE, Sherwood CR (2011) Formation dynamics of subsurface hydrocarbon intrusions following the Deepwater Horizon blowout. *Geophys Res Lett* 38(9):L09602.
2. Diercks AR, et al. (2010) Characterization of subsurface polycyclic aromatic hydrocarbons at the Deepwater Horizon site. *Geophys Res Lett* 37(20):L20602.
3. Joye SB, MacDonald IR, Leifer I, Asper V (2011) Magnitude and oxidation potential of hydrocarbon gases released from the BP oil well blowout. *Nat Geosci* 4(3):160–164.
4. Kessler JD, et al. (2011) A persistent oxygen anomaly reveals the fate of spilled methane in the deep Gulf of Mexico. *Science* 331(6015):312–315.
5. Reddy CM, et al. (2012) Composition and fate of gas and oil released to the water column during the Deepwater Horizon oil spill. *Proc Natl Acad Sci USA* 109(50): 20229–20234.
6. Valentine DL, et al. (2010) Propane respiration jump-starts microbial response to a deep oil spill. *Science* 330(6001):208–211.
7. Camilli R, et al. (2010) Tracking hydrocarbon plume transport and biodegradation at Deepwater Horizon. *Science* 330(6001):201–204.
8. Dubinsky EA, et al. (2013) Succession of hydrocarbon-degrading bacteria in the aftermath of the deepwater horizon oil spill in the gulf of Mexico. *Environ Sci Technol* 47(19):10860–10867.
9. Hazen TC, et al. (2010) Deep-sea oil plume enriches indigenous oil-degrading bacteria. *Science* 330(6001):204–208.
10. Ryerson TB, et al. (2012) Chemical data quantify Deepwater Horizon hydrocarbon flow rate and environmental distribution. *Proc Natl Acad Sci USA* 109(50): 20246–20253.
11. Spier C, Stringfellow WT, Hazen TC, Conrad M (2013) Distribution of hydrocarbons released during the 2010 MC252 oil spill in deep offshore waters. *Environ Pollut* 173: 224–230.
12. McNutt MK, et al. (2012) Review of flow rate estimates of the Deepwater Horizon oil spill. *Proc Natl Acad Sci USA* 109(50):20260–20267.
13. Lu Z, et al. (2012) Microbial gene functions enriched in the Deepwater Horizon deep-sea oil plume. *ISME J* 6(2):451–460.
14. Mason OU, et al. (2012) Metagenome, metatranscriptome and single-cell sequencing reveal microbial response to Deepwater Horizon oil spill. *ISME J* 6(9):1715–1727.
15. Redmond MC, Valentine DL (2012) Natural gas and temperature structured a microbial community response to the Deepwater Horizon oil spill. *Proc Natl Acad Sci USA* 109(50):20292–20297.
16. Schrope M (2013) Dirty blizzard buried Deepwater Horizon oil. *Nature*, 10.1038/nature.2013.12304.
17. Baelum J, et al. (2012) Deep-sea bacteria enriched by oil and dispersant from the Deepwater Horizon spill. *Environ Microbiol* 14(9):2405–2416.
18. Chanton JP, et al. (2012) Radiocarbon evidence that carbon from the Deepwater Horizon spill entered the planktonic food web of the Gulf of Mexico. *Environ Res Lett* 7(4):045303.
19. Cherrier J, Sarkodee-Adoo J, Guilderson TP, Chanton JP (2014) Fossil carbon in particulate organic matter in the Gulf of Mexico following the Deepwater Horizon event. *Environmental Science and Technology Letters* 1(1):108–112.
20. Passow U, Ziervogel K, Asper V, Diercks A (2012) Marine snow formation in the aftermath of the Deepwater Horizon oil spill in the Gulf of Mexico. *Environ Res Lett* 7(3):035301.
21. Kujawinski EB, et al. (2011) Fate of dispersants associated with the deepwater horizon oil spill. *Environ Sci Technol* 45(4):1298–1306.
22. Chakraborty R, Borglin SE, Dubinsky EA, Andersen GL, Hazen TC (2012) Microbial response to the MC-252 oil and Corexit 9500 in the Gulf of Mexico. *Front Microbiol* 3:357.
23. Rivers AR, et al. (2013) Transcriptional response of bathypelagic marine bacterioplankton to the Deepwater Horizon oil spill. *ISME J* 7(12):2315–2329.
24. Valentine DL, et al. (2012) Dynamic autoinoculation and the microbial ecology of a deep water hydrocarbon irruption. *Proc Natl Acad Sci USA* 109(50):20286–20291.
25. Prince RC, et al. (1994) 17.alpha.(H)-21.beta.(H)-hopane as a conserved internal marker for estimating the biodegradation of crude oil. *Environ Sci Technol* 28(1): 142–145.
26. Aeppli C, et al. (2014) Recalcitrance and degradation of petroleum biomarkers upon abiotic and biotic natural weathering of Deepwater Horizon oil. *Environ Sci Technol* 48(12):6726–6734.
27. Liu Y (2011) *Monitoring and Modeling the Deepwater Horizon Oil Spill: A Record-Breaking Enterprise* (American Geophysical Union, Washington, DC), pp vii, 271 pp.
28. Paris CB, et al. (2012) Evolution of the Macondo well blowout: Simulating the effects of the circulation and synthetic dispersants on the subsea oil transport. *Environ Sci Technol* 46(24):13293–13302.
29. Garcia-Pineda O, et al. (2013) Detection of floating oil anomalies from the Deepwater Horizon oil spill with synthetic aperture radar. *Oceanography (Wash DC)* 26(2): 124–137.
30. Le Hénaff M, et al. (2012) Surface evolution of the deepwater horizon oil spill patch: Combined effects of circulation and wind-induced drift. *Environ Sci Technol* 46(13): 7267–7273.
31. Mezić I, Loire S, Fonoberov VA, Hogan P (2010) A new mixing diagnostic and Gulf oil spill movement. *Science* 330(6003):486–489.
32. Lindo-Atichati D, et al. (2014) Simulating the effects of droplet size, high-pressure biodegradation, and variable flow rate on the subsea evolution of deep plumes from the Macondo blowout. *Deep Sea Res Part II Top Stud Oceanogr*, 10.1016/j.dsr1012.2014.1001.1011.
33. Aeppli C, et al. (2012) Oil weathering after the Deepwater Horizon disaster led to the formation of oxygenated residues. *Environ Sci Technol* 46(16):8799–8807.
34. Aeppli C, Reddy CM, Nelson RK, Kellermann MY, Valentine DL (2013) Recurrent oil sheens at the deepwater horizon disaster site fingerprinted with synthetic hydrocarbon drilling fluids. *Environ Sci Technol* 47(15):8211–8219.
35. Carmichael CA, et al. (2012) Floating oil-covered debris from Deepwater Horizon: Identification and application. *Environ Res Lett* 7(1):015301.
36. Mason OU, et al. (2014) Metagenomics reveals sediment microbial community response to Deepwater Horizon oil spill. *ISME J* 8(7):1464–1475.
37. White HK, et al. (2012) Impact of the Deepwater Horizon oil spill on a deep-water coral community in the Gulf of Mexico. *Proc Natl Acad Sci USA* 109(50):20303–20308.
38. Boehm PD, Carragher PD (2012) Location of natural oil seep and chemical fingerprinting suggest alternative explanation for deep sea coral observations. *Proc Natl Acad Sci USA* 109(40):E2647–E2647, author reply E2648.
39. White HK, et al. (2012) Reply to Boehm and Carragher: Multiple lines of evidence link deep-water coral damage to Deepwater Horizon oil spill. *Proc Natl Acad Sci USA* 109(40):E2648–E2648.
40. Fisher CR, et al. (2014) Footprint of Deepwater Horizon blowout impact to deep-water coral communities. *Proc Natl Acad Sci* 111(32):11744–11749.
41. Montagna PA, et al. (2013) Deep-sea benthic footprint of the deepwater horizon blowout. *PLoS ONE* 8(8):e70540, 10.1371/journal.pone.0070540.
42. Burdige DJ (2006) *Geochemistry of Marine Sediments* (Princeton Univ Press, Princeton, NJ).
43. Yeager KM, Santschi PH, Rowe GT (2004) Sediment accumulation and radionuclide inventories (Pu-239,Pu-240, Pb-210 and Th-234) in the northern Gulf of Mexico, as influenced by organic matter and macrofaunal density. *Mar Chem* 91(1-4):1–14.

# Supporting Information

Valentine et al. 10.1073/pnas.1414873111

## Hopane Data Interpolation

The hopane data used in this study represent discrete sample concentrations collected at individual core locations (*Methods*). Estimates of the total amount of hopane deposited in the study area (Fig. 5) were calculated using spatial interpolation methods based on the discrete sample concentration values. All analyses were performed using the Geostatistical Analyst Toolbox in ArcGIS 10.2 and are described below. Additional information about the individual parameters, statistics, and techniques used is available (1).

**Inverse Distance Weighting.** The data were explored first using inverse distance weighting (IDW), a simple interpolator that averages the values of a given number of data points in a specified search neighborhood and weights them by their distance from the interpolated point (1, 2). This technique assumes no stationarity in the data and operates under the assumption that points that are closer to one another are more similar than those farther apart. To this end, the model requires a defined maximum and minimum number of neighboring points, a search neighborhood geometry and radius, and a power function that defines the weight of the neighboring points proportional to their inverse distance. It should be noted that this method by definition preserves the exact value located at the input points where the distance is zero.

In this analysis, a constant circular search radius of 40 km was used, and variation was allowed in the maximum number of points used to interpolate at a given location. Varying the maximum number of points in the interpolation has an effect similar to varying the radius: Using a greater number of points will include points farther away, and using fewer points will, in effect, limit the search radius. An additional geometry also was tested whereby the circular geometry was split into four quadrants with the main axis oriented at a 45° angle. This geometry was chosen for two reasons: (*i*) the elevated hopane data tend to follow a 45° southwest–northeast trend, creating some overall anisotropy as it impinges on the rising topography of the continental slope, and (*ii*) the four quadrants force the interpolation to use the prescribed number of points from each quadrant, preventing spatial selectivity from a cluster of points in a limited region or direction. Last, the power-law exponent was varied using values of 1 and 3, whereby the weights of surrounding points are proportional to the inverse distance from the interpolated point raised to the prescribed exponent. In simple terms, an exponent of 0 would weight all points evenly regardless of distance, but as the exponent increases, the weights of distant points decrease rapidly. Table S1 presents the parameter setups for the IDW interpolation models.

For each IDW model cross-validation was performed. In cross-validation each input point is removed, one at a time, and the surface is interpolated again to predict the associated value using the other points. In lieu of IDW prediction errors, these cross-validation values can be compared with the input point value to obtain a general metric of the model's robustness. Ideally, the mean predicted error from the cross-validation would be close to 0, and the root mean squared error (RMSE) would be as low as possible (i.e., an RMSE and mean predicted error of 0 would be a perfect match between the predicted and the measured data points).

Results from the IDW interpolation over the study area are shown in Table S1. Mean hopane concentrations range from 170–213 $ng{\cdot}g^{-1}$ for individual runs and account for 5.8–7.5% of the total hopane discharge estimate from the Macondo Well. This calculation assumes a background hopane concentration of 28 $ng{\cdot}g^{-1}$ in the Gulf of Mexico and provides one estimate of uncertainty as to the magnitude of hopane contamination in this region. Mean predicted errors and RMSE are relatively insensitive to the range of parameters tested.

**Empirical Bayesian Kriging.** IDW is simplistic and fast, but kriging techniques generally require a considerable amount of decision-making and some assumptions about the stationarity and distribution of data (1, 2). Kriging statistical techniques allow a variety of output surfaces to be produced, including predictions, prediction SEs, probabilities, and quantiles, permitting better constraint and quantification of the errors associated with different parameters and interpolations. In this study, EBK was chosen as the preferred kriging method for several reasons (1, 3, 4). First, EBK automates the most difficult aspects of creating a valid kriging model by subsetting the data and running multiple semivariogram simulations to derive a best fit. This automation reduces the amount of interactive modeling and greatly simplifies the optimization of parameters. Second, EBK provides more accurate estimates of error by accounting for the uncertainty in the semivariogram, whereas other kriging methods assume that the estimated semivariogram is the true semivariogram for the entire interpolation region. Thus, other kriging methods tend to underestimate the SEs of prediction. Last, there is greater flexibility and accuracy in predictions of moderately nonstationary data using EBK than in those using other kriging methods. The primary disadvantage of EBK is that, because it is an iterative method, it can be computationally intensive with larger datasets. This drawback did not prove to be problematic in this study.

Similar to the IDW analysis, the number of maximum and minimum neighbors and the neighborhood geometry were varied. A standard circular geometry with a radius of 40 km was fixed throughout, as were the overlap factor, subset size, and number of semivariogram simulations. The overlap factor specifies the degree of overlap between subsets; at the maximum possible overlap factor of 5, each point can be used in five different simulations, creating a smoother output surface. The subset size was fixed at 20 points to improve computational efficiency and constrain the semivariogram estimate to a smaller area that better captures the inherent variability of the dataset. For each subset, a semivariogram is estimated from the data, and new data are unconditionally simulated at each of the input locations in the subset. A new semivariogram then is estimated from the simulated data and is used again to simulate new data. In this study, this process was repeated 200 times per subset, with the distribution of these simulations providing the improved statistical treatment of errors compared with other methods of interpolation. It should be noted that the overlap factor, subset sizes, and number of simulations were optimized and fixed based on computational efficiency as well as statistical fit, but the varied parameters in Table S2 were the main source of variability in error.

Results from the EBK analysis (Tables S2 and S3) demonstrate similar error statistics across parameter runs and when converted to a surface show mean hopane concentration values similar to those in the IDW analyses (Table S1), ranging from 171–209 $ng{\cdot}g^{-1}$. These concentrations represent 5.8–7.3% of the total estimated hopane released from the Macondo Well and provide a second measure of uncertainty as to the magnitude of hopane contamination in this area. The most statistically robust parameter run was EBK-C (Fig. S6 and Table S4); this

is the preferred prediction dataset used in the article (Figs. 5 and 6) as well as for statistical quantile prediction surfaces (Fig. S6 and Table S4). Ideally, a prediction surface will have a mean error close to 0, a low RMSE and average standard prediction error (these also should be close to each other in value), and a root mean squared standardized prediction error (RMSE Std) close to 1. Because EBK-C has an RMSE Std error of 0.89, it is likely that we are slightly overestimating the variability in the predictions.

### Particle Deposition Modeling

Using R (version 3.0.3), we built a Monte Carlo model of particle deposition in several iterative rounds of parameter fitting. In each run, the model simulates a 2 m × 2 m patch of sediment, determining the locations of $n$ random particles at 1-mm resolution by uniform sampling of integer points on the intervals $x$ = [0, 2,000], $y$ = [0, 2,000]. Particles are treated in terms of the oil masses they carried, making no assumptions about the mass or volume contribution of any nonoil material (e.g., bacterial floc). For each particle, the oil mass was sampled from a broad normal distribution, and the hopane mass fraction was sampled from a normal distribution with a mean of 58 μg hopane·g(oil)$^{-1}$ [SD, 8 μg hopane·g(oil)$^{-1}$], as calculated from the available data released by NOAA.

Next, coring is simulated by randomly choosing a 3,136-mm$^2$ block [the cross-section of a standard 6.35-cm (2.5-in) push-core] within the patch. The number and size of particles caught by each core then are determined, and the surficial hopane concentration signal in nanograms of hopane per gram of sample is determined as follows. First, the background sample mass is determined for a 1-cm-thick section of sediment with a dry weight of 0.38 g·cm$^{-3}$ (*Methods*). Second, for any particles caught by the core, the simulated oil mass and hopane mass fraction are used to calculate the particle-borne hopane mass. Third, the core is assigned a background hopane signal, drawn at random from the distribution of measured background-level (<75 ng·g$^{-1}$) surficial hopane concentrations in the dataset. Finally, the hopane concentration is calculated as the sum of background (adjusted to account for the additional oil mass) and signal (excess hopane mass divided by the sum of dry sediment mass and excess oil mass) concentrations. Note that this calculation is derived from the hopane concentration and does not include the mass of any nonoil components of the particle.

The resulting distribution of simulated surficial hopane concentrations was compared with the distribution measured in 707 cores at 534 sampling sites. In initial fitting, the model permitted a single mean oil mass; repeated rounds of simulation ($10^3$ runs per set of parameters) were used to scan an average of 5 ng–5 g oil per particle and 10–$10^6$ particles per 2 m × 2 m patch (Fig. S2). At particle densities >$10^4$ per patch, cores are very likely to capture at least one particle, leaving too few background-level cores; at lower spatial densities, an oil mass ≤0.25 mg is insufficient to shift the surficial hopane concentration substantially, whereas an oil mass of ∼5 g per particle causes too great a shift, with no way to populate the substantial peak at 100–200 ng·g$^{-1}$. We therefore focused on spatial densities of 10–1,000 particles per patch and oil masses of 3.4 mg–1.8 g. In addition, because no single mean oil mass could regenerate the multimodal form of the observed distribution of surficial hopane concentrations, we moved to a mixed model of relatively common oil-poor particles, less common midrange particles, and rare oil-rich particles. In four successive rounds of $\chi^2$ minimization, we alternated between refining the number and the mean oil mass of each type of particle. The final fitted values (800 particles with a mean oil mass of 0.024 g per 2 m × 2 m patch, 90 particles with a mean oil mass of 0.19 g, and 20 particles with a mean oil mass of 1.13 g) gave $\chi^2$ = 1,934 with 706 degrees of freedom (Fig. S3).

To assess the heterogeneity of surficial hopane concentration signals expected from this model, we simulated sampling two, three, four, or five disjoint cores from each of 10,000 patches (2 m × 2 m) generated using the optimized parameters. As before, we calculated the surficial hopane concentration for each core; in addition, we then calculated the mean and SD of each single-site set of simulated hopane concentrations, obtaining a set of 10,000 paired single-site mean and SD values for two-core simulations, a second set for three-core simulations, a third for four-core simulations, and a fourth for five-core simulations. These values are plotted as black points in Fig. 3; as expected, the distribution becomes more compact as the number of cores per site increases. Finally, we calculated the mean and SD of surficial hopane concentration measurements at each of the 117 sampling sites at which multiple parallel cores were collected and compared these observations (red points in Fig. 3) with the simulation.

### Background Hopane Concentration

To define hopane contamination from the *Deepwater Horizon* event, an estimate of background hopane concentration was needed. A search of published literature and government reports failed to provide prespill hopane concentrations for surficial sediments in the northeast Gulf of Mexico. Therefore, on the assumption that surficial hopane concentrations measured close to the well are more likely to reflect contamination, and distant measurements are more likely to reflect the regional background, the regional distribution of surficial hopane was analyzed with respect to distance from the Macondo Well. This analysis shows that mean surficial hopane concentration decreases as distance increases to 40 km but remains roughly constant at 28 ± 23 ng·g$^{-1}$ at greater distances ($n$ = 70), suggesting that 28 ng·g$^{-1}$ represents the regional mean background concentration of hopane in surficial sediments (Fig. S4). This approach likely provides an upper estimate of the background concentration, because some of the samples collected at distances >40 km may have been contaminated with low concentrations of Macondo oil. The mean background estimate of 28 ng·g$^{-1}$ shows little sensitivity to the distance threshold chosen so long as the distance is greater than 40 km (Fig. S4).

The calculated mean background concentration was consistent with several patterns observed within 40 km of the Macondo Well. (*i*) Hopane's sediment depth distribution revealed that sediment collected beneath the surface layer typically was within the range observed for surficial samples collected >40 km from the well (e.g., Fig. 2). (*ii*) Surficial hopane concentrations within the background range are present within 40 km of the Macondo Well, as is consistent with some proximal areas receiving lesser inputs of oil. (*iii*) Clusters of samples within the 40-km radius are within the background range; notably, for samples collected at a water depth >1,700 m the mean surficial hopane concentration (±SD) was 51.7 (±34.5) ng·g$^{-1}$ ($n$ = 47). Although not conclusive, these observations are broadly consistent with our estimate of 28 ng·g$^{-1}$ as a reasonable choice of mean background concentration.

To calculate the excess hopane in the vicinity of the Macondo Well, the mean background concentration (28 ng·g$^{-1}$) was subtracted from the total calculated mean concentration in the contaminated region (170–213 ng·g$^{-1}$; see *Inverse distance weighting*, above). The mean concentration of surficial hopane within 40 km of the Macondo Well is substantially higher than the background value of 28 ng·g$^{-1}$, and thus the calculation of excess hopane is relatively insensitive to small changes in the background concentration.

In addition to the mean background surficial hopane concentration, we sought to establish a cutoff value that could be used to determine with high confidence whether a given sample is marked by contamination with Macondo oil. The surficial hopane concentration is <75 ng·g$^{-1}$ in >95% of samples

collected outside the 40-km contamination radius (Fig. S4); therefore we used 75 ng·g$^{-1}$ as a threshold value and considered higher measurements as showing evidence of likely contamination. Some patterns in the data emerge at higher threshold concentrations (e.g., 100 ng·g$^{-1}$ in Fig. 2*B*), presumably because the signal from Macondo oil begins to dominate background variability.

## Accessing NRDA Data

The data used in this study were downloaded from www.gulfspillrestoration.noaa.gov/oil-spill/gulf-spill-data/ on January 1, 2014. The data were identified by the category of sediment and were located under the radio button titled "NRDA data by category."

## Limitations of This Study

In this study, we argue that the observed hopane anomaly is caused by discharged Macondo oil; that the observed anomaly implies deposition of ∼12% (range 4–31%) of the oil trapped in deep intrusion layers to the sea floor; and that the observed anomaly is best explained by the deposition of a heterogeneous range of oil-bearing particles from the intrusion layers. Each of these arguments carries caveats. First, no hydrocarbon has been shown to be unique to Macondo oil, to permit definitive identification of discharged Macondo oil. Instead, our identification is based on the spatial distribution of the hopane anomaly, which is best explained by a point source at the Macondo Well. In the absence of any reasonable alternative, we consider this interpretation to be robust and advance this argument with a high degree of certainty. Second, our estimates of the extent of hopane contamination in the study area entail the propagation of multiple uncertainties and could be biased toward the low side by the necessary exclusion of several potential hopane reservoirs (as discussed in the main text). We therefore view these calculations with a moderate degree of certainty and consider our final estimate to be a likely lower bound. Third, although available information is consistent with our proposed mechanism for the deposition of oil from the deep intrusion layers to the sea floor, the data are insufficient to make a robust conclusion. We present this mechanism with a low degree of certainty.

The determination of error in the scaling calculation propagates uncertainties in several parameters (as described in the main text), including the hopane concentration in Macondo oil, sediment porosity, total oil discharge to the deep ocean, and the background hopane concentration. We include no explicit estimate of error for the assumed volume of the contaminated area or the assumed sediment density; furthermore, we were unable to assess analytical error for individual hopane measurements used to calculate the average contamination level, typically on the order of 10–20%. In addition to our preferred EBK estimate (and the associated error based on these assumptions), we suggest that the estimate should be bounded at the low end by the lowest EBK estimate minus one SD and at the high end by the highest EBK estimate plus one SD (Table S3).


1. ArcGIS Online Help 10.2. Environmental Systems Research Institute, Inc. (ESRI). http://resources.arcgis.com/en/help/main/10.2/). Accessed February 10, 2014.
2. Webster R, Oliver MA (2007) *Geostatistics for Environmental Scientists* (John Wiley & Sons, Ltd., West Sussex).
3. Chilès J-P, Delfiner P (1999) *Geostatistics: Modeling Spatial Uncertainty* (John Wiley & Sons, Inc., New York).
4. Pilz J, Spöck G (2008) Why do we need and how should we implement Bayesian kriging methods. *Stochastic Environ Res Risk Assess* 22(5):621–632.

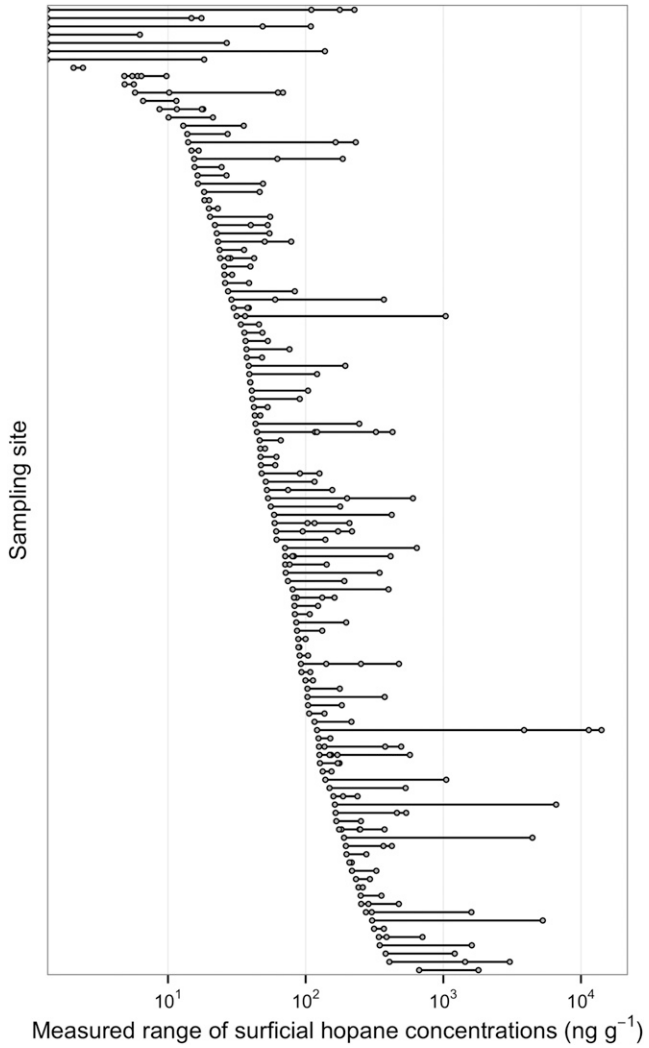


**Fig. S1.** Meter-scale lateral variability in surficial hopane concentrations measured in multiple parallel cores. Sets of two, three, four, or five cores were collected in parallel at 117 sampling sites; sites are ordered on the *y* axis by minimum reported surficial hopane concentration, and all measurements for a given site's cores are shown as gray points. Note that the *x* axis is on a log scale.

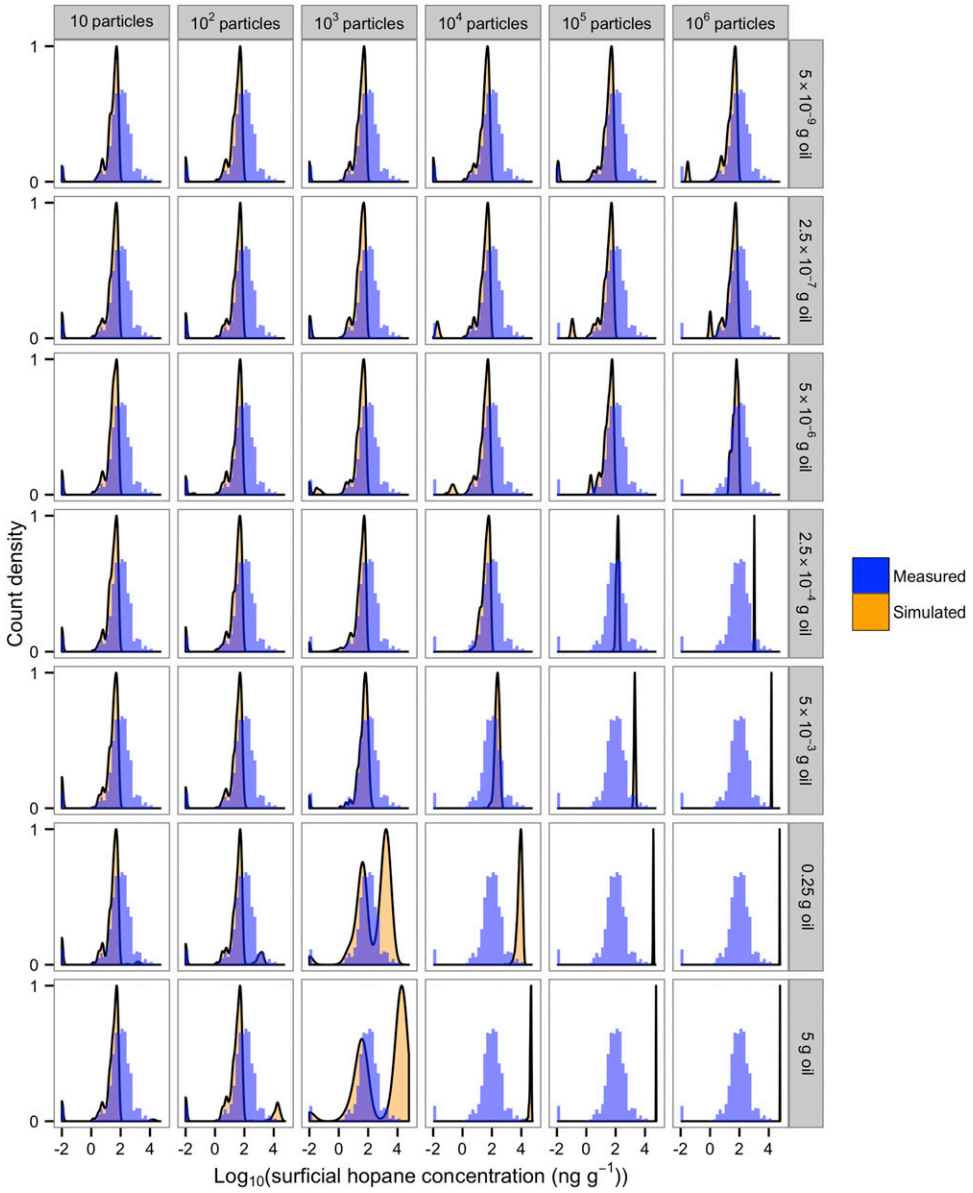


**Fig. S2.** Results of the initial round of particle deposition model fitting, demonstrating that the distribution of measured surficial hopane concentrations is not well fitted by a model in which particle spatial density is high or in which particle sizes cluster around a single value. Model refinement proceeded to investigate a combination of particles bearing small (~0.02 g), medium (~0.2 g), and large (~1 g) oil masses at decreasing probabilities.

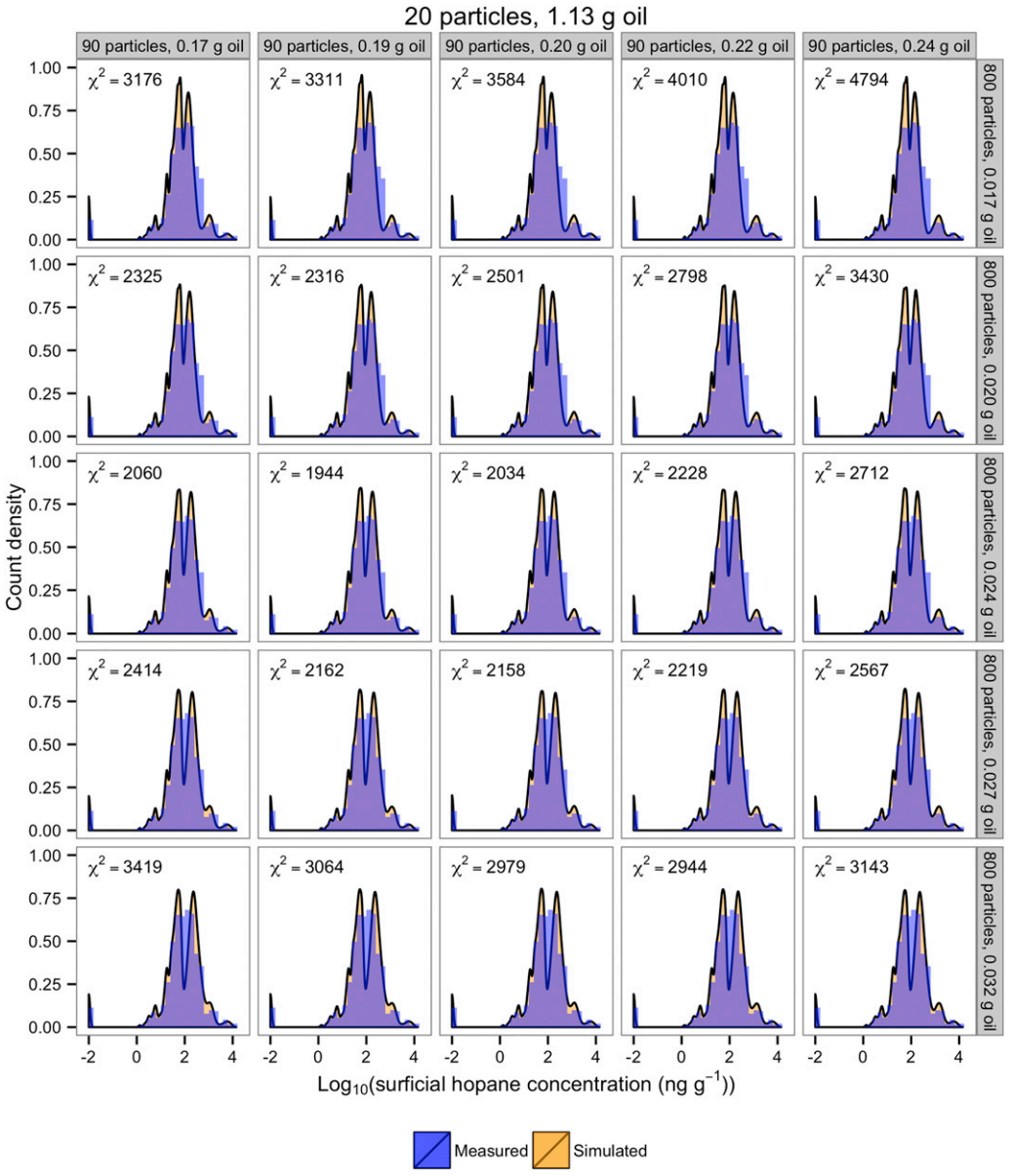


**Fig. S3.** Results of the final round of particle deposition model fitting, showing only the results for the optimal value of 1.13 g oil per oil-rich particle. $\chi^2$ minimization identified the successful model as containing 800 oil-poor (mean oil mass, 0.024 g), 90 medium (mean oil mass, 0.19 g), and 20 oil-rich (mean oil mass, 1.13 g) particles per 2 m × 2 m patch of sediment.

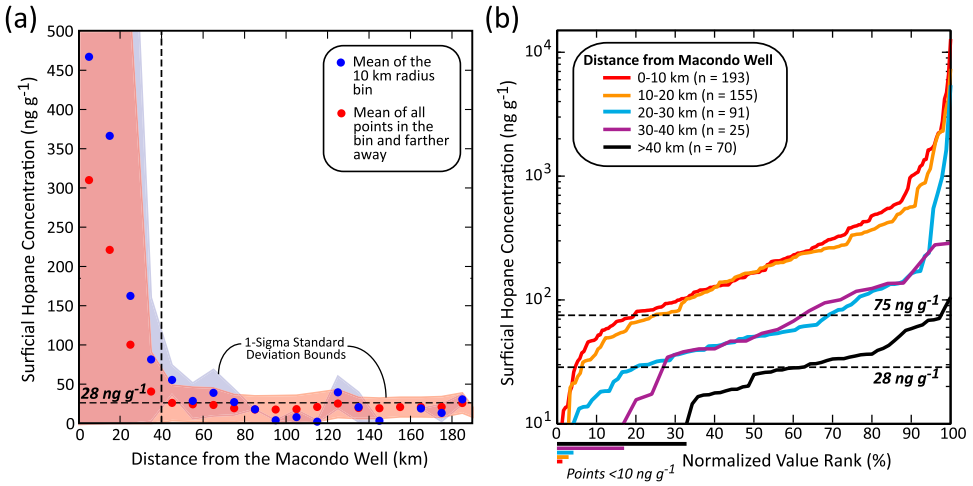


**Fig. S4.** Relationships between surficial hopane concentration and distance from the Macondo Well highlighting the empirically derived background value of 28 ng·g$^{-1}$. (*A*) Mean hopane concentrations calculated in 10-km radial bins (blue dots) from the Macondo Well along with the evolving mean concentration (red dots), which is calculated using the data from the given bin along with data from all more distal bins. Red and blue envelopes correspond to the respective colored points and indicate ±1 SD about the means. The background hopane value of 28 ng·g$^{-1}$ is derived from the mean of the data >40 km distant from the Macondo Well as indicated by the vertical line. (*B*) Normalized rank plot for five individual bins showing decreasing hopane values with increasing distance from the source. Note that the background hopane concentration of 28 ng·g$^{-1}$ is greater than ∼60% of the points found in the >40-km distance bin.

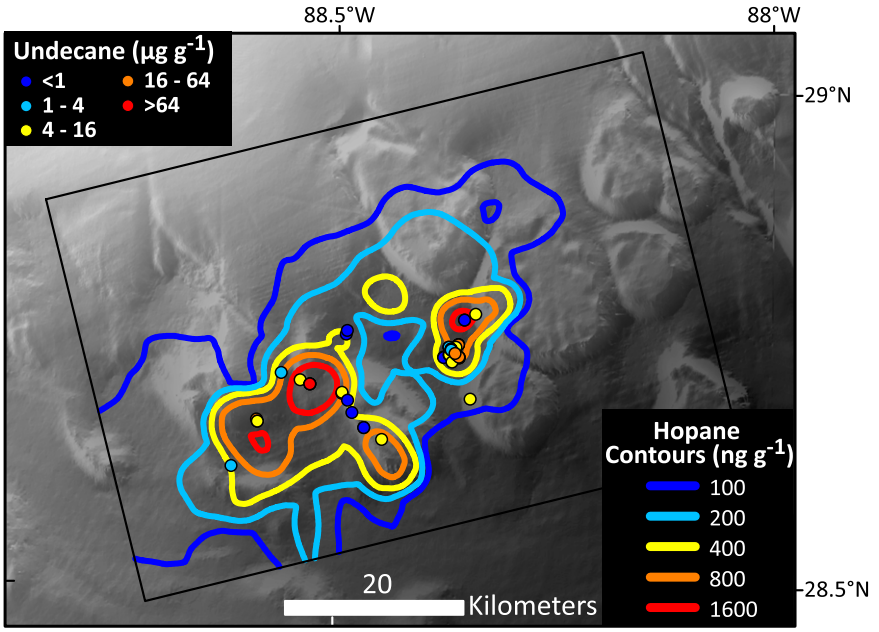


**Fig. S5.** Concentration of undecane ($n$ = 51) overlaid on the interpolated hopane contours and study area as in Fig. 6*B* in the main text.

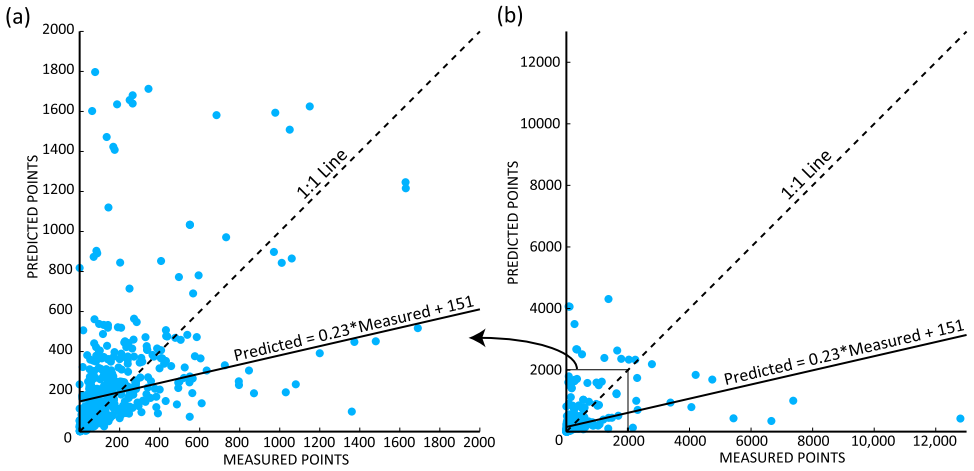


**Fig. S6.** EBK-C cross-validation plot zoomed in (*A*) and with all data (*B*), showing the line of best fit. Fit statistics are provided in Table S5.

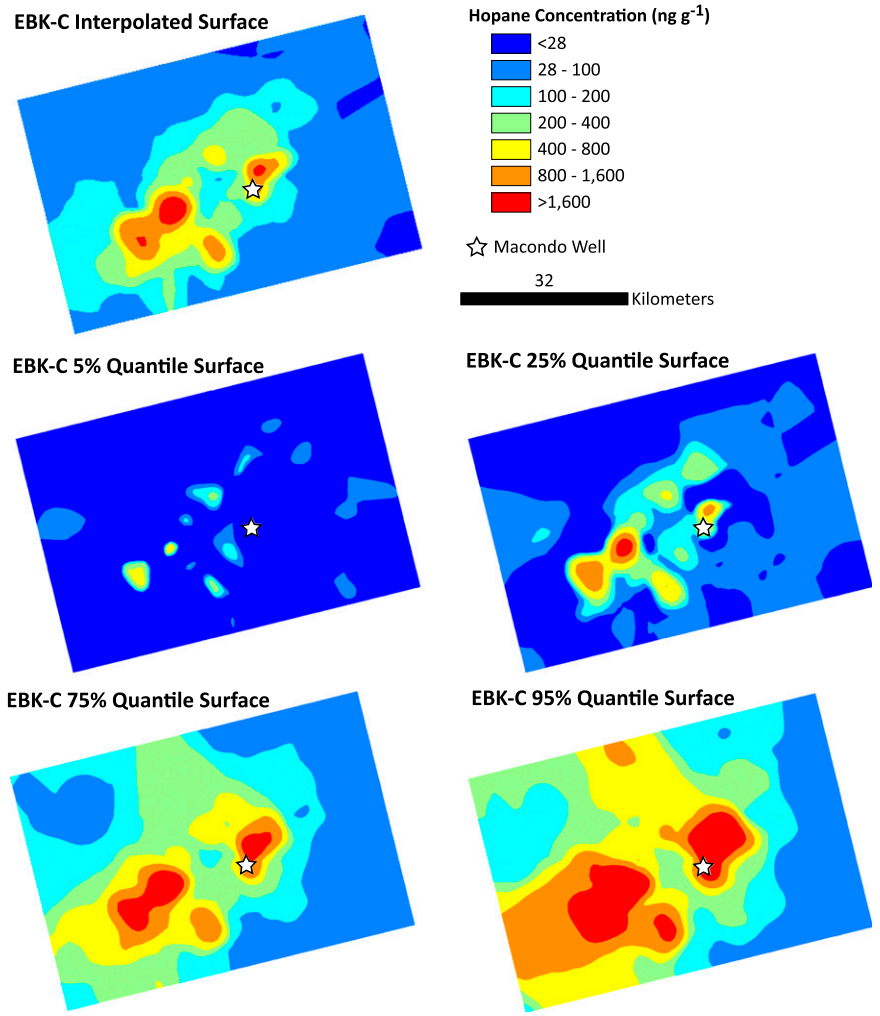


**Fig. S7.** EBK-C interpolated prediction surface and quantile prediction surfaces smoothed using a 2-km circular smoothing kernel for enhanced viewing. Statistics are provided in Table S4.

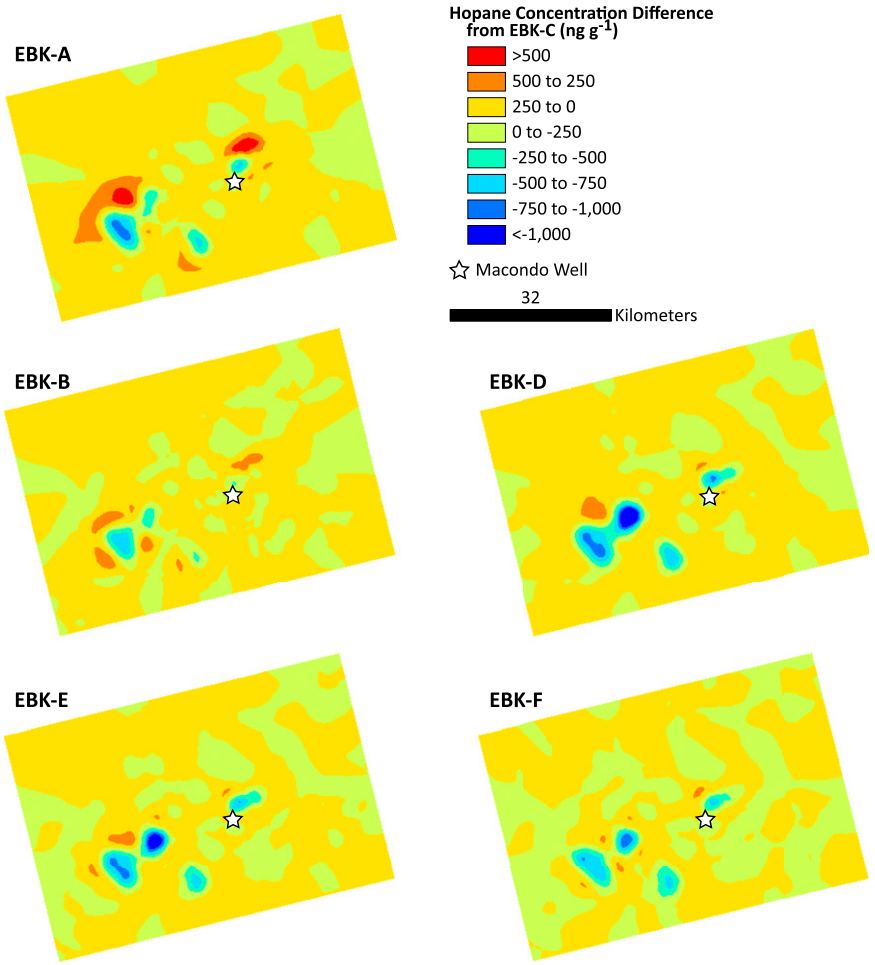


**Fig. S8.** Interpolated surface concentration differences between EBK-C and EBK-A through EBK-F smoothed using a 2-km circular smoothing kernel for enhanced viewing. Positive values indicate higher concentrations than EBK-C, and negative values indicate lower concentration values than EBK-C.

**Table S1. IDW interpolation surface parameters and results using a 40-km radius standard circular search neighborhood**

| ID | Power | Maximum no. of neighbors | Minimum no. of neighbors | Sector type | RMSE | Mean error* | Mean hopane, $ng \cdot g^{-1}$† | % total hopane‡ |
|---|---|---|---|---|---|---|---|---|
| IDW-A | 1 | 20 | 10 | 1 sector | 996 | 33.1 | 213 | 7.5 |
| IDW-B | 3 | 20 | 10 | 1 sector | 1,059 | 20.8 | 184 | 6.3 |
| IDW-C | 1 | 5 | 3 | 1 sector | 1,022 | 18.4 | 174 | 5.9 |
| IDW-D | 3 | 5 | 3 | 1 sector | 1,058 | 14.6 | 170 | 5.8 |
| IDW-E | 1 | 10 | 5 | 4 sectors at 45° | 976 | 24.6 | 203 | 7.1 |
| IDW-F | 3 | 10 | 5 | 4 sectors at 45° | 1,058 | 20.8 | 184 | 6.3 |
| IDW-G | 1 | 5 | 3 | 4 sectors at 45° | 990 | 20.3 | 181 | 6.2 |
| IDW-H | 3 | 5 | 3 | 4 sectors at 45° | 1,057 | 17.6 | 175 | 6.0 |

*Mean prediction error from cross validation.

†Mean hopane concentration inside the defined study area (Fig. 5).

‡Percent of the total estimated hopane discharged from the Macondo Well calculated using the mean hopane value minus the estimated background value of 28 $ng \cdot g^{-1}$.

**Table S2. EBK interpolation surface parameters and cross-validation statistics using a 40-km radius standard circular search neighborhood, an overlap factor of 5, and a subset size of 20 points with 200 semivariogram simulations per subset**

| ID | Maximum no. of neighbors | Minimum no. of neighbors | Sector type | Mean* | Mean Std† | RMSE | RMSE Std | Average SE‡ |
|---|---|---|---|---|---|---|---|---|
| EBK-A | 20 | 10 | 1 sector | 12.1 | 0.03 | 817 | 0.77 | 932 |
| EBK-B | 10 | 5 | 1 sector | 14.2 | 0.03 | 811 | 0.83 | 923 |
| EBK-C | 5 | 3 | 1 sector | 4.1 | 0.02 | 881 | 0.89 | 954 |
| EBK-D | 10 | 5 | 4 sectors at 45° | 5.3 | 0.02 | 812 | 0.69 | 932 |
| EBK-E | 5 | 3 | 4 sectors at 45° | −4.0 | 0.02 | 803 | 0.71 | 914 |
| EBK-F | 3 | 2 | 4 sectors at 45° −8.1 | −8.1 | 0.02 | 827 | 0.76 | 904 |

*Mean prediction error.
†Mean standardized prediction error.
‡Average standard prediction error.

**Table S3. EBK hopane concentration interpolation results from the study area**

| ID | Mean, ng·g$^{-1}$* | Maximum, ng·g$^{-1}$ | Minimum, ng·g$^{-1}$ | SD, ng·g$^{-1}$ | % total hopane† |
|---|---|---|---|---|---|
| EBK-A | 209 | 5,976 | 20 | 321 | 7.3 |
| EBK-B | 192 | 6,118 | 16 | 337 | 6.6 |
| EBK-C | 179 | 6,020 | 15 | 370 | 6.1 |
| EBK-D | 184 | 2,945 | 19 | 218 | 6.3 |
| EBK-E | 175 | 3,477 | 7 | 249 | 6.0 |
| EBK-F | 171 | 4,228 | 16 | 281 | 5.8 |

*Mean hopane concentration inside the defined study area (Fig. 5).
†Percent of the total estimated hopane discharged from the Macondo Well calculated using the mean hopane value minus the background value of 28 ng·g$^{-1}$.

**Table S4. Sample points ($n$ = 461) and EBK-C hopane concentration interpolation quantile results from the study area**

| Quantile | Mean, ng·g$^{-1}$* | Maximum, ng·g$^{-1}$ | Minimum, ng·g$^{-1}$ | SD, ng·g$^{-1}$ | % total hopane† |
|---|---|---|---|---|---|
| Points | 355 | 12,800 | 0 | 931 | 13.2 |
| 5% | <0 | 3,632 | <0 | 428 | 0.0 |
| 25% | 53 | 5,270 | <0 | 278 | 1.0 |
| Mean | 179 | 6,020 | 15 | 370 | 6.1 |
| 75% | 306 | 7,336 | 17 | 514 | 11.3 |
| 95% | 587 | 9,060 | 33 | 841 | 22.6 |

*Mean hopane concentration inside the defined study area (Fig. 5).
†Percent of the total estimated hopane discharged from the Macondo Well calculated using the mean hopane value minus the background value of 28 ng·g$^{-1}$.

**Table S5. Estimates of pure oil droplet aggregation necessary to produce particles bearing the oil masses fitted in the particle deposition model**

| Oil mass, g | No. of droplets with a 25-μm radius | No. of droplets with a 50-μm radius |
|---|---|---|
| 0.02 | $4.4 \times 10^5$ | $5.5 \times 10^4$ |
| 0.19 | $3.5 \times 10^6$ | $4.4 \times 10^5$ |
| 1.1 | $1.9 \times 10^7$ | $2.4 \times 10^6$ |

## Other Supporting Information Files

Dataset S1 (XLS)